A Mutation in *Syne2* Causes Early Retinal Defects in Photoreceptors, Secondary Neurons, and Müller Glia

Dennis M. Maddox,[1] Gayle B. Collin,[1] Akihiro Ikeda,[2] C. Herbert Pratt,[1] Sakae Ikeda,[2] Britt A. Johnson,[2,3] Ron E. Hurd,[1] Lindsay S. Shopland,[1] Jürgen K. Naggert,[1] Bo Chang,[1] Mark P. Krebs,[1] and Patsy M. Nishina[1]

[1]The Jackson Laboratory, Bar Harbor, Maine, United States
[2]University of Wisconsin-Madison, Department of Medical Genetics, Madison, Wisconsin, United States
[3]University of Miami, Miller School of Medicine, Miami, Florida, United States

Correspondence: Patsy M. Nishina, The Jackson Laboratory, 600 Main Street, Bar Harbor, ME 04609, USA; patsy.nishina@jax.org.

DMM, GBC, and AI contributed equally to the work presented here and should therefore be regarded as equivalent authors.

Submitted: November 10, 2014
Accepted: April 27, 2015

Citation: Maddox DM, Collin GB, Ikeda A, et al. A mutation in *Syne2* causes early retinal defects in photoreceptors, secondary neurons, and Müller glia. *Invest Ophthalmol Vis Sci*. 2015;56:3776–3787. DOI:10.1167/iovs.14-16047

Purpose. The purpose of this study was to identify the molecular basis and characterize the pathological consequences of a spontaneous mutation named cone photoreceptor function loss 8 (*cpfl8*) in a mouse model with a significantly reduced cone electroretinography (ERG) response.

Methods. The chromosomal position for the recessive *cpfl8* mutation was determined by DNA pooling and by subsequent genotyping with simple sequence length polymorphic markers in an F2 intercross phenotyped by ERG. Genes within the candidate region of both mutants and controls were directly sequenced and compared. The effects of the mutation were examined in longitudinal studies by light microscopy, marker analysis, transmission electron microscopy, and ERG.

Results. The *cpfl8* mutation was mapped to Chromosome 12, and a premature stop codon was identified in the spectrin repeat containing nuclear envelope 2 (*Syne2*) gene. The reduced cone ERG response was due to a significant reduction in cone photoreceptors. Longitudinal studies of the early postnatal retina indicated that the cone photoreceptors fail to develop properly, rod photoreceptors mislocalize to the inner nuclear layer, and both rods and cones undergo apoptosis prematurely. Moreover, we observed migration defects of secondary neurons and ectopic Müller cell bodies in the outer nuclear layer in early postnatal development.

Conclusions. SYNE2 is important for normal retinal development. We have determined that not only is photoreceptor nuclear migration affected, but also the positions of Müller glia and secondary neurons are disturbed early in retinal development. The *cpfl8* mouse model will serve as an important resource for further examining the role of nuclear scaffolding and migration in the developing retina.

Keywords: *cpfl8*, development, migration defect, retina, *Syne2*

SYNE2 (formerly Nesprin 2 and NUANCE), the second reported member of a family of giant scaffolding proteins,[1] is an ortholog of the *Drosophila melanogaster* muscle protein Msp-300.[2] SYNE2 is a component of the linker of nucleoskeleton and cytoskeleton (LINC) complex and is reported to localize to the outer nuclear membrane where it plays a role in connecting the nucleus to the cytoskeleton.[3] The amino-terminal calponin homology domains of SYNE2 interact with filamentous actin in the cytosol, whereas its carboxy-terminal conserved Klarsicht, ANC-1, Syne homology (KASH) domain anchors the protein at the nuclear envelope.[4] The LINC complex, which also includes emerin, SYNE1, SUN1, SUN2, and lamin A, serves in mechanostructural, signaling and gene regulatory roles in the cell.[5] Functional defects in SYNE2 in humans lead to development of Emery-Dreifuss muscular dystrophy as well as dilated cardiomyopathy.[6] Targeted null mutations in mice have been shown to affect motor neuron innervation and respiration[7] and cause a progeria-like skin phenotype.[8] Although not reported in human patients, KASH and SUN domain proteins have been implicated in ocular abnormalities in *Drosophila* and in zebrafish. In *Drosophila*, loss of klarsicht (KASH protein homolog) or klaroid (SUN gene homolog) leads to aberrant nuclear migration of photoreceptor nuclei.[9,10] Likewise in zebrafish, retinal overexpression of a truncated form of *Syne2a* lacking the KASH domain also results in mislocalization of photoreceptor nuclei.[11,12] Subsequent studies of *Syne2* null mouse mutants have reported microcephaly, behavioral abnormalities, and aberrant retinal development including early nuclear migration defects.[7,13,14]

In the developing retina, interkinetic nuclear migration (INM) is a process by which nuclei of neuroepithelial progenitor cells migrate within the neuroblastic layer (NBL), in coordination with the cell cycle, between the apical and basal surfaces.[15,16] Although the purpose of INM is not fully understood, mutations in a number of genes that encode LINC complex proteins, including *Syne2*, have been shown to disrupt the proper migration of nuclei during development of the retina[13,17] and other cell types in tissues such as muscle.[6]

SYNE2 is highly expressed in developing and adult retinas.[18] Early in development, the KASH-specific isoform of SYNE2 localizes homogenously to the nuclear envelope rims throughout the NBL. As the retina matures, expression of the large

KASH-specific isoform of SYNE2 is downregulated and undetectable at the photoreceptor nuclear rims. However, *Syne2* expression is observed in the photoreceptor inner segments, inner nuclear layer, and ganglion cell layer of adult retinas by in situ analysis.

Here we demonstrated that, like the *Syne2*$^{-/-}$ null mutant,[13] homozygous *Syne2*^{cpfl8} mice also exhibit an abnormal cone and rod electroretinography (ERG) phenotype and pan-retinal photoreceptor degeneration. Furthermore, we determined that the reduction in cone ERG response results not only from the cell death reported previously[13] but, more significantly, from the lack of proper cone development. We also reported a novel finding that horizontal as well as bipolar cells migrate abnormally and form ectopic synapses that may contribute to the observed reduced b-wave amplitudes. In addition, a subset of Müller glial cells also appeared to migrate improperly.

Methods

Identification and Maintenance of Mutant Mice

The recessive *cpfl8* mutation arose on a B6.129S7-*Ifngr1*^{tm1Agt}/J background. *cpfl8* founders were identified by an abnormal cone ERG response pattern and were backcrossed to C57BL/6J (B6) mice for several generations to remove the targeted *Ifngr1* mutation. Subsequently, the colony was maintained through intercross matings of affected siblings.

Syne2^{cpfl8} homozygotes and B6 control mice used in this study were maintained under a 12L:12D cycle. Autoclaved NIH-31 diet (6% fat, 18% protein, Ca:P 1:1, vitamin and mineral fortified; PMI, Richmond, IN, USA) and HCl-acidified water (pH 2.8–3.2) were provided ad libitum. Mice were housed in groups of four or five in polycarbonate boxes of 51 in^2 area on bedding of sterilized shavings (northern white pine; Hancock Lumber, Fryeburg, ME, USA). All mice were treated in accordance with protocols approved by The Jackson Laboratory Animal Care and Use Committee and in compliance with the Association for Research in Vision and Ophthalmology statement for ethical care and use of animals.

Genetic Mapping

To determine the map position of the *cpfl8* mutation, homozygous mice were outcrossed to strain DBA/2J, and the resulting F1 progeny were intercrossed. F2 progeny were evaluated by light-adapted ERG for cone photoreceptor function. DNA samples from 15 affected and 11 unaffected F2 mice were pooled and genotyped with simple sequence length polymorphic markers across all chromosomes (Fine Mapping Facility; The Jackson Laboratory, Bar Harbor, ME, USA). For fine mapping of the critical region, homozygous B6(129S7)-*cpfl8/Pjn* mice were outcrossed to C3.B6-*Pde6b*$^+$ mice, and F1 mice were intercrossed. A total of 251 F2 progeny were phenotyped by ERG analysis and genotyped for single nucleotide polymorphic markers to refine the critical region.

Sequencing

Pairs of eyes enucleated from adult *cpfl8* mutants (n = 3) and wild-type mice (n = 3) were homogenized with a Virtishear tissue homogenizer (SP Industries, Warminster, PA, USA) for 2 minutes on ice in Trizol solution (Invitrogen, Life Technologies, Carlsbad, CA, USA). RNA was isolated according to the manufacturer's directions, and the total RNA quality was assessed by electrophoresis of a 5-mL aliquot of each RNA sample on a 1% agarose gel. RNA samples were reverse transcribed into cDNA with a RETROscript kit (Ambion, Life Technologies). Complementary DNA of mutants and controls was amplified by PCR and sequenced with oligonucleotide primers specific for the candidate genes (DNA Sequencing Facility, The Jackson Laboratory). All genes within the critical region were completely sequenced. Data were analyzed with MacVector version 7.2.3 software (MacVector, Inc., Cary, NC, USA) and Sequencher version 4.2 software (Gene Codes Corp., Ann Arbor, MI, USA).

Electroretinography

Full-field ERG recordings were performed as described by Nusinowitz et al.[19] Briefly, anesthesia was induced by intraperitoneal injection of a mixture of ketamine (70 mg/kg) and xylazine (15 mg/kg), and body temperature (36.5°C to 37°C) was maintained with a temperature-controlled heating pad. A gold loop electrode was placed on the surface of the cornea and referenced to a gold wire placed in the mouth. A needle electrode placed in the tail served as ground. Signals were amplified (×10,000; CP511 AC amplifier; Grass Instruments, Warwick, RI, USA), sampled at 0.8-ms intervals and averaged. Dark-adapted responses were recorded to short wavelength (λ_{max} = 470 nm; Wratten 47A filter) strobe flashes over a 5.0 log unit range. Light-adapted responses were obtained using white flashes superimposed on a steady rod-saturating adapting field (32 cd/m^2) after a 10-minute period of light adaptation. Responses were averaged at all intensities, and up to 50 records were averaged for the weakest signals. A signal rejection protocol was used to eliminate electrical artifacts produced by blinking and eye movements.

Western Blot Analysis

Postnatal day 4 eyes from B6 control and *Syne2*^{cpfl8} homozygous mice were homogenized in 100 µL radioimmunoprecipitation assay buffer (RIPA buffer; 1% NP40, 0.5% sodium deoxycholate, 0.1% SDS in phosphate buffered saline) containing protease inhibitor cocktail (Roche Diagnostics, Indianapolis, IN, USA). Protein concentrations were determined using a Direct Detect spectrophotomer (EMD Millipore, Darmstadt, Germany); and 40 µg total protein from each sample was loaded with lithium dodecyl sulfate (LDS) sample buffer and reducing agent (NuPAGE; Life Technologies). Samples were electrophoresed on 3% to 8% precast gels with Tris acetate in XT Tricine buffer (Criterion XT; Bio-Rad Laboratories, Inc., Hercules, CA, USA). Samples were transferred overnight onto a 0.45-µm polyvinylidene fluoride membrane (GE Healthcare, Wauwatosa, WI, USA), and the membrane was blocked for 1 hour in 5% milk powder in 0.05% Tween in Tris-buffered saline (TBS-T) before being probed with a polyclonal antibody against human SYNE2 (1:200 dilution in 4% bovine serum albumin in TBS-T; Abnova Antibodies, Walnut, CA, USA). The epitope of this antibody corresponds to residues 6687 to 6784 immediately upstream of the KASH domain in murine SYNE2 (GenBank reference sequence NP_001005510). After being washed 3× in TBS-T, the membrane was probed with a peroxidase-conjugated anti-mouse secondary antibody (1:2000 dilution; Bio-Rad Laboratories), and signal was detected with Supersignal West Pico chemiluminescent reagent (ThermoFisher Scientific, Suwanee, GA, USA).

Histology and Immunofluorescence of Paraffin-Embedded Retinas

For light microscopy, retinas were fixed in a solution of 37.5% methanol/12.5% glacial acetic acid in (0.5×) phosphate-buffered saline (PBS), embedded in paraffin, and sectioned at 6-µm

Investigative Ophthalmology & Visual Science

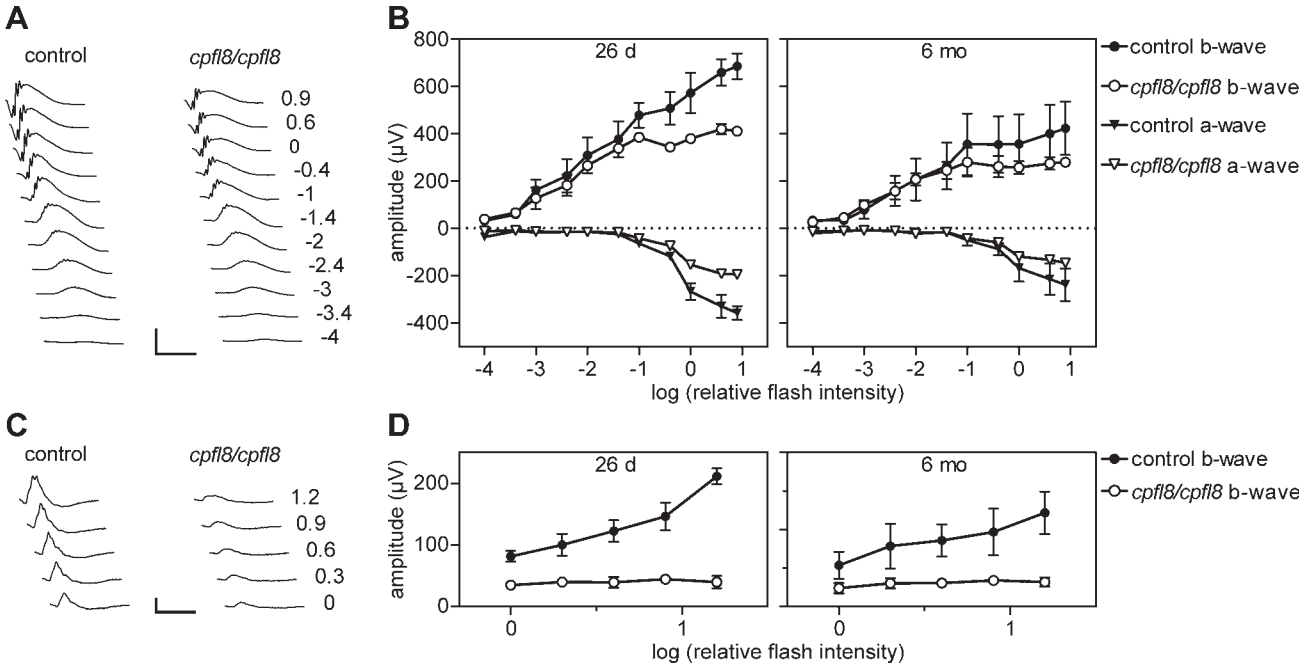

Figure 1. Full-field scotopic (**A**, **B**) and phototopic (**C**, **D**) ERG responses recorded at postnatal day 26 (26 d) and 6 months (6 mo) in representative *cpfl8* mutants and B6 controls. (**A**) Averaged traces at P26 are shown. *Scale bar*: 500 μm vertical, 100 ms horizontal. (**B**) Electroretinograms of rods at 26 days and 6 months. Rod function in *cpfl8* homozygotes is reduced at 26 days and 6 months relative to that of controls. (**C**) Averaged traces at 26 days show significant loss of cone function in homozygous *cpfl8* retinas. *Scale bar*: 100 μm vertical, 100 ms horizontal. (**D**) Electroretinograms of cones at 26 days and 6 months. Cone responses are similar between sampled time points, indicating no progressive cone function loss with age. (B6, $n = 3$–5; *cpfl8/cpfl8*, $n = 3$.) The log of the relative intensity is shown in each *graph*; a value of 0 corresponds to a flash lamp output of 14.8 cd/m^2.

intervals. Sections were subsequently mounted on Superfrost Plus slides (Fisher Scientific, Pittsburgh, PA, USA) and stained with hematoxylin and eosin. For immunohistochemistry, sections were cut from paraffin-embedded retinas fixed in 4% paraformaldehyde and mounted directly onto Superfrost plus slides (Fisher Scientific). Prior to being labeled with antibody, sections were deparaffinized in xylene and hydrated through a series of ethanol gradients and incubated in PBS. For cryostat sections, eyes were fixed in 4% paraformaldehyde for 2 hours at 4°C, then cryoprotected at 4°C in a series of graded sucrose. Eyes were embedded in OCT at −20°C, using a cryoembedding system (Precision, Wyckoff, NJ, USA) and sectioned at 12-μm thicknesses. For immunohistochemistry, sections were blocked in PBS with 0.5% Triton X-100 and 2% normal donkey or horse serum for 20 minutes at room temperature. Sections were then incubated at 4°C overnight in primary antibody diluted in blocking solution. Sections were then rinsed in PBS and incubated in a secondary antibody/blocking solution for 45 minutes at room temperature. Antibody control slides were made by omitting the primary antibody to demonstrate the absence of staining (data not shown). Primary antibodies included anti-cleaved caspase-3 (Cell Signaling Technologies, Inc., Danvers, MA, USA), anti-VGLUT1 (Synaptic Systems, Goettingen, Germany), anti-mGluR6 (Neuromics, Edina, MN, USA), anti-CTBP2 (Santa Cruz Biotechnology, Inc., Dallas, TX, USA), anti-CRALBP (kind gift from JC Saari, University of Wisconsin), anti-IBA1 (Wako, Richmond, VA, USA), anti-histone-H3 (phospho S-10), anti-PKC-α, calbindin (Abcam, Cambridge, MA, USA), anti-blue opsin, CHX10, anti-synaptophysin (Santa Cruz Biotechnology), anti-red/green opsin, and anti-recoverin, (Chemicon, EMD Millipore). Appropriate secondary antibodies were coupled to either Cy3 (Jackson ImmunoResearch, Inc., Westgrove, PA, USA) and diluted 1:200, or Alexa-488 (Molecular Probes, Life Technologies) and diluted 1:200. Adult mice 1 to 3 months of age were used for examination of the spatial expression of retinal proteins. For developmental studies, samples were tested at postnatal days (P) 0, P2, P5, P8, and P14 and at 1 and 6 months. Slides were imaged on a DMLB upright microscope (Leica, Wetzlar, Germany) using Q Imaging software (Q Imaging, Surrey, BC, Canada), an inverted microscope with Apotome (Carl Zeiss Meditec AG, Berlin, Germany) using Zen software, or a Radiance 2100 rainbow confocal laser scanning system on a model TE2000 (Nikon, Minato-ku, Tokyo, Japan) inverted microscope using Lasersharp 2000 software (Bio-Rad Laboratories).

For retinal whole mounts, eyes were fixed in cold 4% paraformaldehyde for 30 minutes. Corneas and lenses were removed, and retinas were cut radially to flatten the tissue. Whole mounts were blocked in 20% serum in PBST solution (0.2%) for 1 hour and labeled with blue cone opsin (1:200 dilution) or red/green opsin (1:200 dilution) for 12 to 18 hours at 4°C. Tissues were washed in PBS and incubated in Cy3-conjugated secondary antibody and fluorescein-labeled peanut agglutinin (PNA) in 10% serum in PBST for 3 hours. Confocal microscopy was performed with a DM6000B model confocal microscope (Leica) using a 63×/1.40 oil immersion objective. Brightness and contrast of confocal images were optimized with Photoshop version 7.0 software (Adobe, San Jose, CA, USA).

For quantitation of cleaved caspase 3 staining, manual segmentation in Fiji software[20] with the wand tool set at 50 was used to create a mask of the NBL. The red channel was thresholded to 80, and the total area of particles from 5 to infinity pixels was determined within the NBL mask. To determine the area fraction of cleaved caspase 3–positive objects, the area of the particles was divided by the area of the mask.

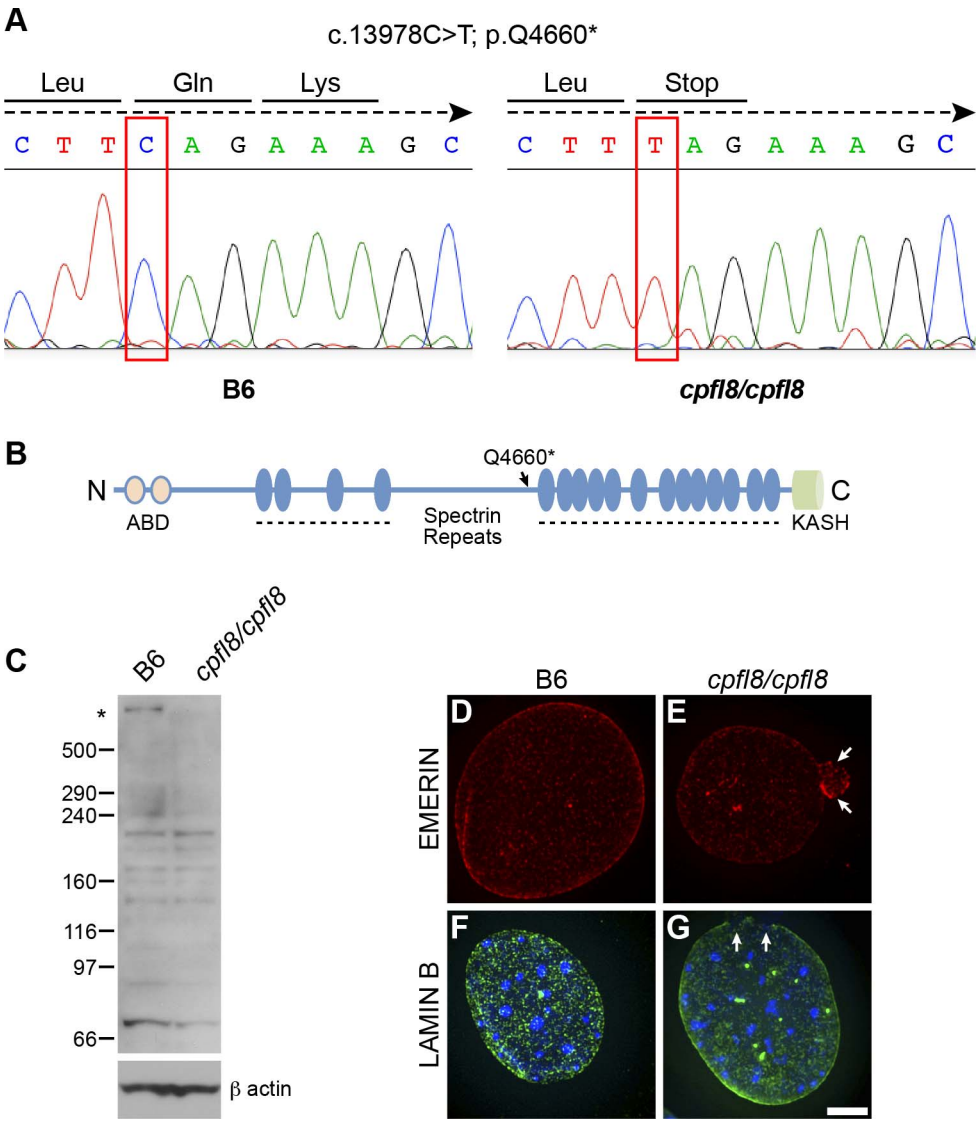

Figure 2. *cpfl8* mutants carry a mutation in *Syne2*, and their cultured fibroblasts display aberrant nuclear morphology. (**A**) Chromatograms showing the transversion observed in *Syne2* in the anti-sense (C>T) strand (chr12:76029898,GRCm38/mm10) of homozygous *Syne2*^{cpfl8} mice. The mutation c.13978C>T; p.Q4660*, results in a nucleotide change of C>T, which replaces glutamine (Q) with a premature stop codon (*) in exon 74. (Note: Mutation position was numbered beginning at the start site [ATG] of the GenBank accession number NM_001005510 open reading frame.) (**B**) Protein structure of SYNE2 showing the positions of the N-terminal actin binding domains (ABD), spectrin repeats, and C-terminal KASH transmembrane domain. Location of the affected residue Q4660* caused by the nonsense mutation is shown. (**C**) Western blot analysis with anti-SYNE2 shows that *Syne2*^{cpfl8} mutant eyes at postnatal day 4 lack the large, ~780 kDa isoform of SYNE2. Smaller immunoreactive bands, present in both control and mutant lysates, may represent other isoforms of SYNE2 thought to be upregulated during the early stages of retinogenesis.[18] (**D**–**G**) Representative fibroblast nuclei are shown from B6 controls (**D**, **F**) and *Syne2*^{cpfl8} homozygotes (**E**, **G**) stained with emerin (EMD [**D**, **E**]) and lamin B (LMNB [**F**, **G**]) antibodies. *Syne2*^{cpfl8} fibroblasts showed variations in nuclear blebbing at the nuclear envelope (*white arrows*). *Scale bar*: 2 μm.

Electron Microscopy

Two-month-old mice were deeply anesthetized and perfused transcardially with a fixative solution of 2% paraformaldehyde/2.5% glutaraldehyde in 0.1 M Sorensen's phosphate buffer, pH 7.4, for 11 minutes. Eyecups were immersion fixed in the same solution for 3 hours at room temperature and stained with 2% OsO_4, followed by dehydration in a graded series of acetone. Samples were then washed with propylene oxide and infiltrated with an increasing proportion of Spurr's low viscosity resin to propylene oxide up to 100% Spurr's. Specimens were infiltrated with 100% Spurr's using a PELCO 3451 Lab microwave system (Ted Pella, Inc., Redding, CA, USA). The resin was then polymerized for 24 hours at 60°C. All sectioning was performed on a Reichert Ultracut E microtome (Reichert/Leica Microsystems, Wetzlar, Germany). Semithin sections were stained with toluidine blue and examined for correct orientation. Subsequently, ultrathin sections were cut with a Microstar type SU diamond knife (Microstar Technologies, Huntsville, TX, USA). Ultrathin sections were stained en drop with uranyl acetate and lead citrate at 60°C. Sections were imaged on a CM120 model scanning transmission electron microscope (Philips Electron Optics, Eindoven, The Nether-

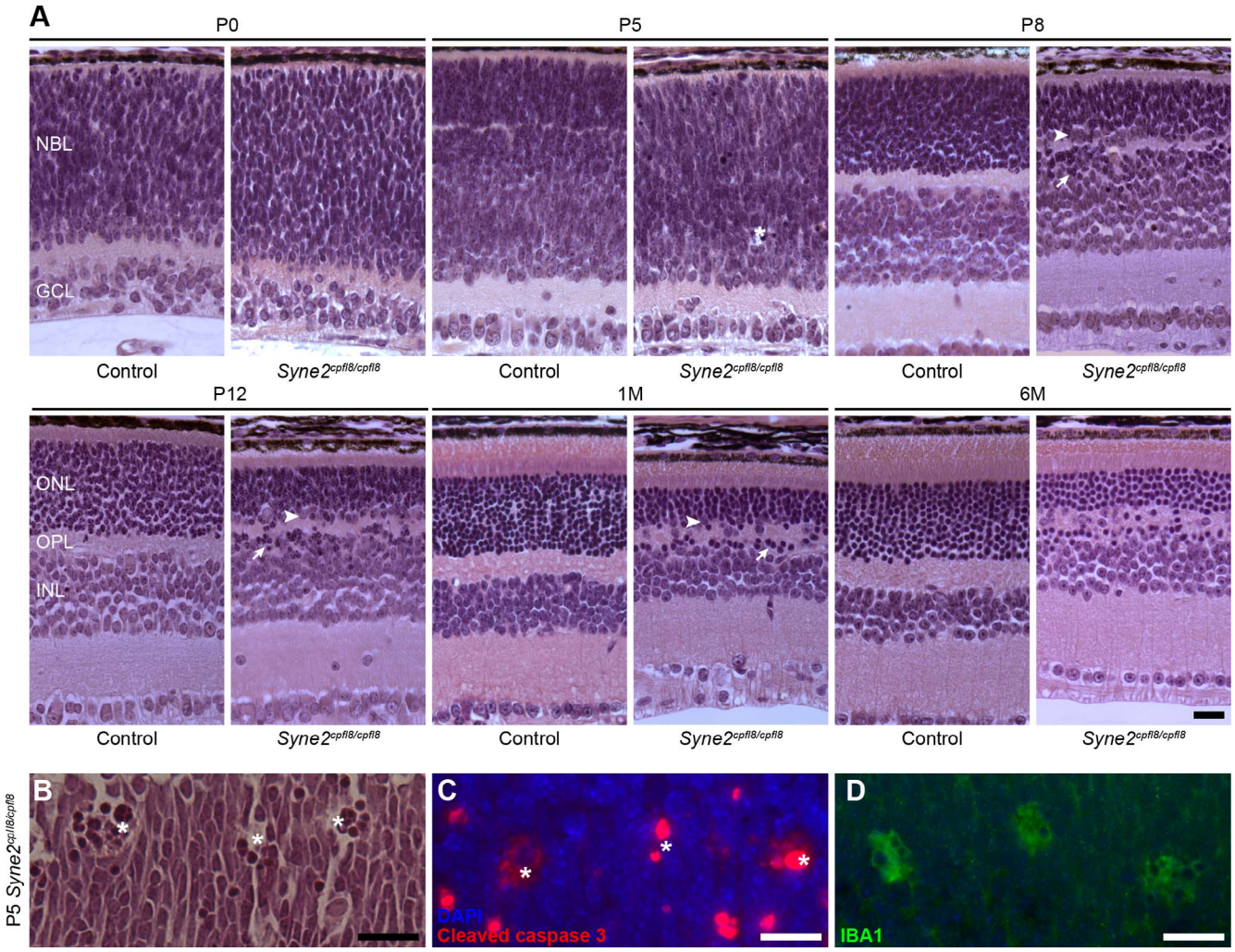

Figure 3. Improper lamination and disruption of the outer plexiform layer are observed in *Syne2*^{cpfl8} homozygotes. (**A**) Longitudinal histological analysis of B6 and *Syne2*^{cpfl8} homozygotes at postnatal days 0, 5, 8, and 12 and at months 1, and 6 (P0, P5, P8, P12, 1M, 6M). Several dense hematoxylin-stained nuclei (*arrow*) similar to those found within the ONL were found ectopically in the OPL and INL of *Syne2*^{cpfl8} mutants. We hypothesize these are mislocalized photoreceptors. *White arrowheads* indicate other displaced neurons within the ONL/OPL. NBL, neuroblast layer; INL, inner nuclear layer; OPL, outer plexiform layer; ONL, outer nuclear layer. (**B**) Magnified view (×40) of the pyknotic nuclei (*asterisks*) observed in *Syne2*^{cpfl8} homozygotes at P5. (**C**, **D**) Immunolabeling of homozygous *Syne2*^{cpfl8} retinas at P5 with apoptotic marker, cleaved caspase 3 ([**C**], *red*), and microglial marker IBA1 ([**D**], *green*) shown in adjacent sections. *Scale bars*: 20 μm.

lands) using Analysis Software (Soft Imaging System Corp., Lakewood, CA, USA).

Cell Culture

Dorsal trunk skin was excised from adult mice and cut into 2- × 2-mm pieces. Subcutaneous tissue was carefully removed, and skin sections were briefly washed in ice-cold, sterile 1× PBS. Skin explants from one mouse were placed dermal side down in a plastic 100-mm culture dish and covered with a sterilized 22- × 22-mm glass coverslip. Dulbecco's modified Eagle's medium (Gibco Life Technologies) supplemented with 10% fetal bovine serum (Lonza BioWhittaker, Allendale, NJ, USA) and 2% antibiotic-antimycotic (Gibco Life Technologies) was added to the culture dish, and cells were cultured at 37°C in a humidified 5% CO_2 incubator for 4 to 7 days to allow fibroblast outgrowth from explants. After 7 days, skin explants were removed, and adherent fibroblasts were passaged with 0.25% Trypsin/1 mM EDTA (Gibco Life Technologies) and plated on sterile 22-mm glass coverslips for analysis.

Nuclear Morphometry

Truncal skin fibroblast nuclei were double-labeled with goat anti-lamin A (Santa Cruz Biotechnology), anti-lamin B (Santa Cruz Biotechnology), and rabbit anti-emerin (Leica Biosystems, Buffalo Grove, IL, USA) antibodies (1:100 dilution) and detected by donkey anti-goat AlexaFluor 488 and rhodamine-conjugated anti-rabbit secondary antibodies (1:200 dilution), respectively (Molecular Probes, Eugene, OR, USA). Three-dimensional images of skin fibroblast nuclei were acquired using an Axiovert 200M model inverted microscope equipped with a Plan-Apochromat 100×/1.40 oil objective (Carl Zeiss Microimaging, Inc., Thornwood, NJ, USA) along with an ORCA-ER digital camera (Hamamatsu, Bridgewater, NJ, USA). Optical sections were acquired at 200-nm intervals. Three-dimensional wide-field epifluorescence images were deconvolved using AutoDeblur software (Media Cybernetics, Bethesda, MD, USA). Single optical sections through the middle of each cell nucleus were evaluated for nuclear membrane blebbing.

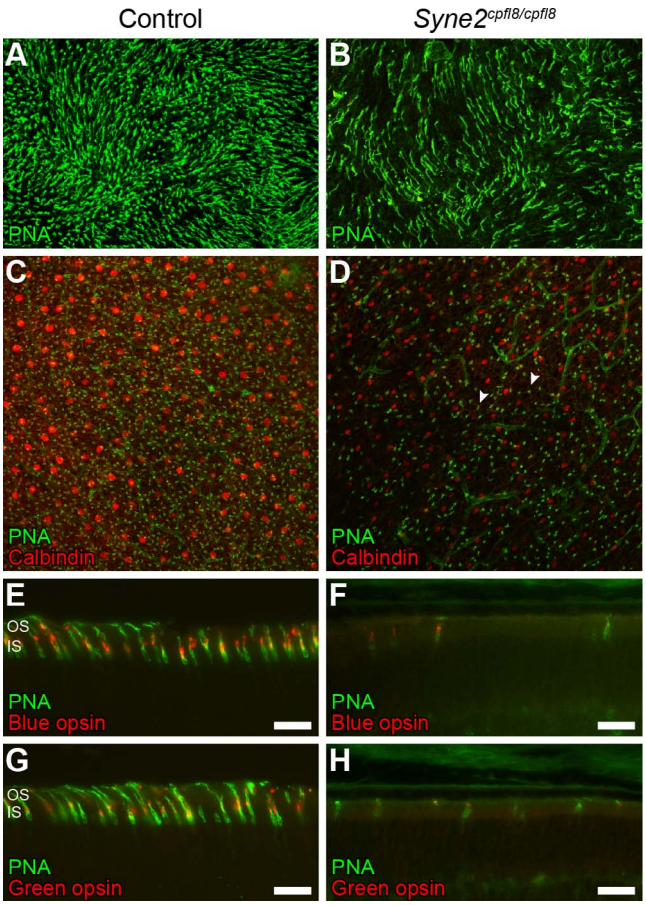

Figure 4. Cone photoreceptors are reduced in number in *Syne2*^{cpfl8} homozygotes. Peanut agglutinin staining (*green*) in wild-type (**A**) and *Syne2*^{cpfl8} (**B**) homozygote flat mounts indicate a reduced number of cone photoreceptors in *Syne2*^{cpfl8} mutants. Cone synaptic terminals (*white arrowhead*) stained with PNA (*green*) were present but were greatly reduced in number in *Syne2*^{cpfl8} homozygotes (**D**) compared to those in B6 controls (**C**). Horizontal cell somata are shown by anti-calbindin staining (*red*). (**E**–**H**) P14 dorsal retinal sections stained with PNA (*green*) and blue opsin ([**E**, **F**], *red*) and green opsin ([**G**, **H**], *red*) show a reduction of both M-cones and S-cones in *cpfl8* mutants (**F**, **H**) compared to those in age-matched controls (**E**, **G**). OS, outer segment; IS, inner segment. *Scale bar*: 20 μm.

Results

cpfl8 Mutation Leads to a Reduction in Cone and Rod ERG Responses

The recessive *cpfl8* mutation was identified from an ongoing screen of retired breeder mice at the Jackson Laboratory for defects in cone ERG response. The mutation arose on a B6.129S7-*Ifngr1*^{tm1Agt}*/J* background but did not cosegregate with the targeted mutation, suggesting that it was caused by an independent spontaneous mutation. As an abnormally low cone ERG response was the phenotype used to detect the mutant, the mutation was named cone photoreceptor function loss 8 (*cpfl8*). The *cpfl8* mutation was moved to the C57BL/6J (B6) background by a series of backcrosses and intercrosses for at least 10 generations. To evaluate the disease progression, we assessed retinal rod and cone ERGs in mice at 26 days and 6 months of age. At 26 days, ERG recordings showed a substantially diminished cone b-wave ERG response and a reduced rod ERG response compared to those of age-matched controls (Fig. 1). No significant changes in implicit times were observed. At 6 months, similarly decreased ERG responses were observed compared to controls, suggesting that the photoreceptor function does not progressively decline as the mice age.

cpfl8 Maps to Mouse Chromosome 12 and Cosegregates With a Nonsense Mutation in the *Syne2* Gene

A genome-wide scan of F2 intercross progeny revealed a critical region of 21.2 Mb on Chromosome 12, flanked by the markers *D12Mit190* (60.8 Mb) and *D12Mit5* (82.0 Mb), which cosegregated with the abnormal cone ERG response. After examining known polymorphisms within this region between B6 and other mouse strains, we selected the C3.B6-*Pde6b*$^{+}$*/J* strain as a mapping partner to generate a fine structure map of the critical region. From a B6(129S7)-*cpfl8* homozygous female × C3.B6-*Pde6b*$^{+}$ homozygous male intercross, we generated 251 F2 mice (502 meioses) that were phenotyped by ERG and genotyped with flanking markers (Supplementary Fig. S1A). After we analyzed the genotypes of informative recombinant mice and progeny testing of noninformative crossover mice, a critical interval of 1.81 Mb was identified between flanking markers rs13481533 (74.79Mb) and rs13481542 (76.59Mb) (Ensembl, Mouse Build 3).

The minimal chromosomal region identified by recombinant mapping for *cpfl8* on Chromosome 12 contained 19 transcripts; a subset, representing the most plausible candidate genes are listed in Supplementary Figure S1B. The entire coding region of all transcripts mapping within the interval was sequenced. Only one transcript, *Syne2*, demonstrated a nonsynonymous sequence variation (Fig. 2A), a C>T transversion in exon 74 (Chr12:76029898,GRCm38/mm10). This single nucleotide mutation, c.13978C>T; p.Q4660*, results in an early translation termination signal in *Syne2* in the long spectrin repeat stretch upstream of the KASH transmembrane domain (Fig. 2B). The mutation results in the absence of the high-molecular-weight isoform (predicted, ~780 kDa) in the P4 *cpfl8* mutant whole-eye lysates, as shown by Western analysis using a C-terminal-specific antibody against SYNE2 (Fig. 2C). Henceforth, the *cpfl8* mutation is designated *Syne2*^{cpfl8}.

Nuclear Morphology Is Irregular in Truncal Skin Fibroblasts of *Syne2*^{cpfl8} Homozygotes

To further corroborate the premature stop codon in the *Syne2* gene as the causative mutation for the aberrant ERG phenotype observed in *cpfl8* mutants, we examined phenotypic characteristics that might be present if *Syne2* were mutated. It is well documented that mutations in nuclear proteins (including *SYNE2*) result in malformations of the nuclear envelope.[8,10,21] Therefore, we cultured and examined truncal skin fibroblasts from B6 and *cpfl8* mice by immunocytochemistry to determine whether the *cplf8* allele of *Syne2* had a similar effect. When labeled with an antibody for the nuclear envelope protein emerin, fibroblast nuclei from B6 mice demonstrated a plump, round appearance, with emerin localized evenly throughout the nuclear envelope (Fig. 2D). In contrast, nuclei in emerin-labeled homozygous *Syne2*^{cpfl8} fibroblasts varied in size and demonstrated increased blebbing at the nuclear envelope (Fig. 2E). The percentage of blebbed nuclei was significantly increased in the mutant (26% in *Syne2*$^{cpfl8/cpfl8}$ compared to 11% in B6, $P < 0.05$). Staining for nuclear lamin B protein gave results similar to those seen for emerin in B6 (Figs. 2D, 2F) and homozygous *Syne2*^{cpfl8} (Figs. 2E, 2G) fibroblasts. Thus, the *Syne2*^{cpfl8} mutation causes nuclear envelope malformation, consistent with altered SYNE2 function.

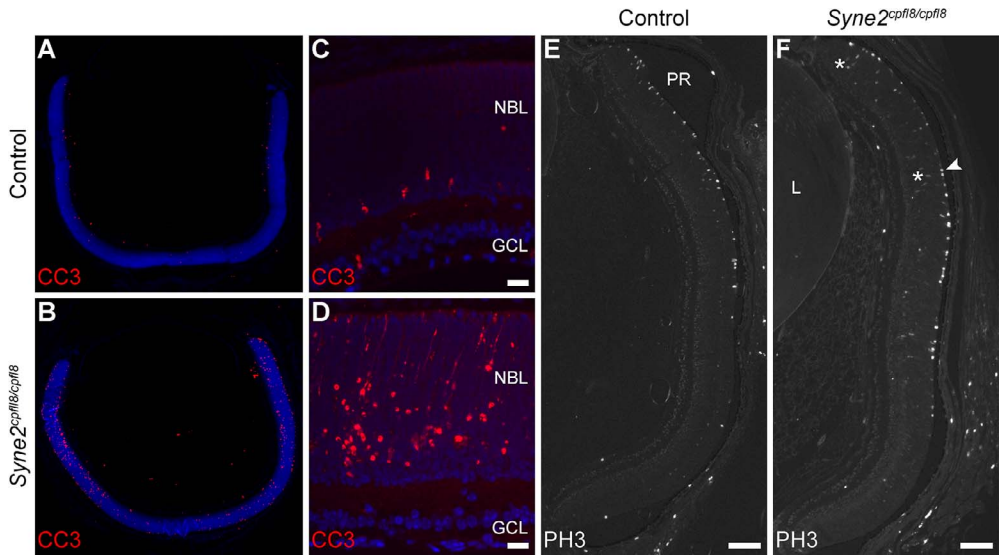

Figure 5. (**A**, **B**) Representative montage of anticleaved caspase 3 (cc3; *red*) staining shows an increased number of apoptotic cells in homozygous *Syne2*^{cpfl8} retinas in comparison to those in B6 controls at P5. Lens autofluorescence was masked manually. Quantitation of cc3 staining revealed a significant increase in cc3 area fraction in the neuroblastic layer in *Syne2* mutants compared to those in B6 controls at P5 (5.1-fold; $P = 0.00042$). $n = 5$ for *Syne2*$^{cpfl8/cpfl8}$; $n = 4$ for B6. (**C**, **D**) Higher magnification of (**A**, **B**). *Scale bar*: 20 μm. (**E**, **F**) Anti-phosphohistone (PH3) staining shows a similar number of proliferating cells in the apical ventricular zone of *Syne2*^{cpfl8} mutant retinas in comparison to those in controls. Phospho-histone H3 positive cells at the basal end of the NBL are shown by *asterisks*. Neuroblast (NBL) and ganglion cell (GCL) layers are shown by DAPI (*blue*) staining of nuclei. *Arrowhead* indicates the apical ventricular zone. Orientation of section is shown where the periphery (PR) is at the *top*. L, lens. *Scale bar*: 100 μm.

Histological Examination Reveals Ectopic Secondary Neurons and Synapses of Homozygous *Syne2*^{cpfl8} Retinas

To determine whether the retinal architecture was perturbed in mice homozygous for the *cpfl8* allele (*Syne2*$^{cpfl8/cpfl8}$), we examined hematoxylin and eosin–stained histological sections throughout retinal development of the *cpfl8* mutant and B6 control mice (Fig. 3A). The first identifiable defect was observed P5. In B6 controls, early signs of synapse formation prominent in the NBL were absent from homozygous *Syne2*^{cpfl8} retinas. By P8, the NBL of control mice was clearly delineated into inner nuclear layer (INL), outer plexiform layer (OPL), and outer nuclear layer (ONL), whereas the OPL in *Syne2*^{cpfl8} homozygotes was not properly developed. At P12, although the OPLs in wild-type retinas were readily discernible, the OPLs of homozygous *Syne2*^{cpfl8} mutants were markedly thinned, and ectopic cells were evident throughout the retina. In the mutant retinas, ectopic cells with nuclei resembling photoreceptor nuclei were found in the INL, whereas other displaced neurons were observed in the ONL. These ectopic cells remained in retinas of adult mice at 1 and 6 months of age. Thicknesses of the INL, ONL, and inner segment (IS) and outer segment (OS) layers were visibly reduced in 1-month-old homozygous mutant retinas compared to controls. The number of photoreceptor nuclear layers in 1-month old mutants remained similar to those in 6-month-old mutants, supporting the ERG findings that the numbers of photoreceptors do not decline with age.

At P5, cells with pyknotic nuclei were observed in the basal region of the NBL of the *Syne2*^{cpfl8} homozygotes but not in wild-type retinas (Fig. 3B). These cells were immunoreactive with cleaved caspase-3 antibody, indicating these cells were undergoing apoptosis (Fig. 3C). In addition, immunolabeling with IBA1 (AIF1), a marker for cells of myeloid lineage, suggested mobilization of retinal microglia and/or infiltrating macrophages around these pyknotic cells (Fig. 3D).

Reduction in Cone Cell Number in *cpfl8* Mutants Results Primarily From Improper Cone Development and Increase in Cell Death

As the mutation in *Syne2*^{cpfl8} was identified in an ERG screen for abnormal cone function, we investigated if cone cells were absent in *cpfl8* mutants or if they were present but functioning poorly. Fluorescent labeling of the cone OS sheaths with PNA in retinal flat mounts showed that there was a large reduction of cone photoreceptors in homozygous *Syne2*^{cpfl8} retinas compared to those in wild-type controls (Figs. 4A, 4B). PNA-labeled cone synaptic terminals were observed in the mutants, but they were greatly reduced in number in comparison to those in wild-type mice (Figs. 4C, 4D). In dorsal sections, PNA staining of cone sheaths was abundant in P14 wild-type retinas but sparse in homozygous *Syne2*^{cpfl8} retinas (Figs. 4E–H).

To determine the time course of the reduction of cones in homozygous *Syne2*^{cpfl8} retinas, we conducted a marker analysis from birth to P14 using an immunohistochemical approach (Figs. 5, 6). Apoptotic cells, detected with anti-caspase-3 staining, were more abundant in homozygous *Syne2*^{cpfl8} retinas than in wild-type age-matched controls as early as P0 (not shown) and peaked at P5 (5.1-fold increase, $P = 0.00042$) (Figs. 5A–D). Anti-phosphohistone 3 (PH3) staining revealed that the distribution of mitotic cells at the apical ventricular surface (Figs. 5E, 5F) in mutant retinas was similar to that in controls; however, elongated PH^{+} cells were observed at the basal end of the NBL of mutant retinas, indicating defects in interkinetic migration. Immunostaining using anti-recoverin (a marker for photoreceptors) showed significantly fewer photoreceptors in *Syne2*^{cpfl8} homozygotes at P5 than in wild-type retinas (Figs. 6A, 6B). Mutant photoreceptors did not form the elongated axonal terminals at P5 as observed in control retinas. We confirmed that these photoreceptors were cones by coexpression with blue opsin, a marker for M-cones (Figs. 6C, 6D). However, because of the reduced number of cone photoreceptors during development and the significant apoptotic loss of photoreceptors prior to

Investigative Ophthalmology & Visual Science

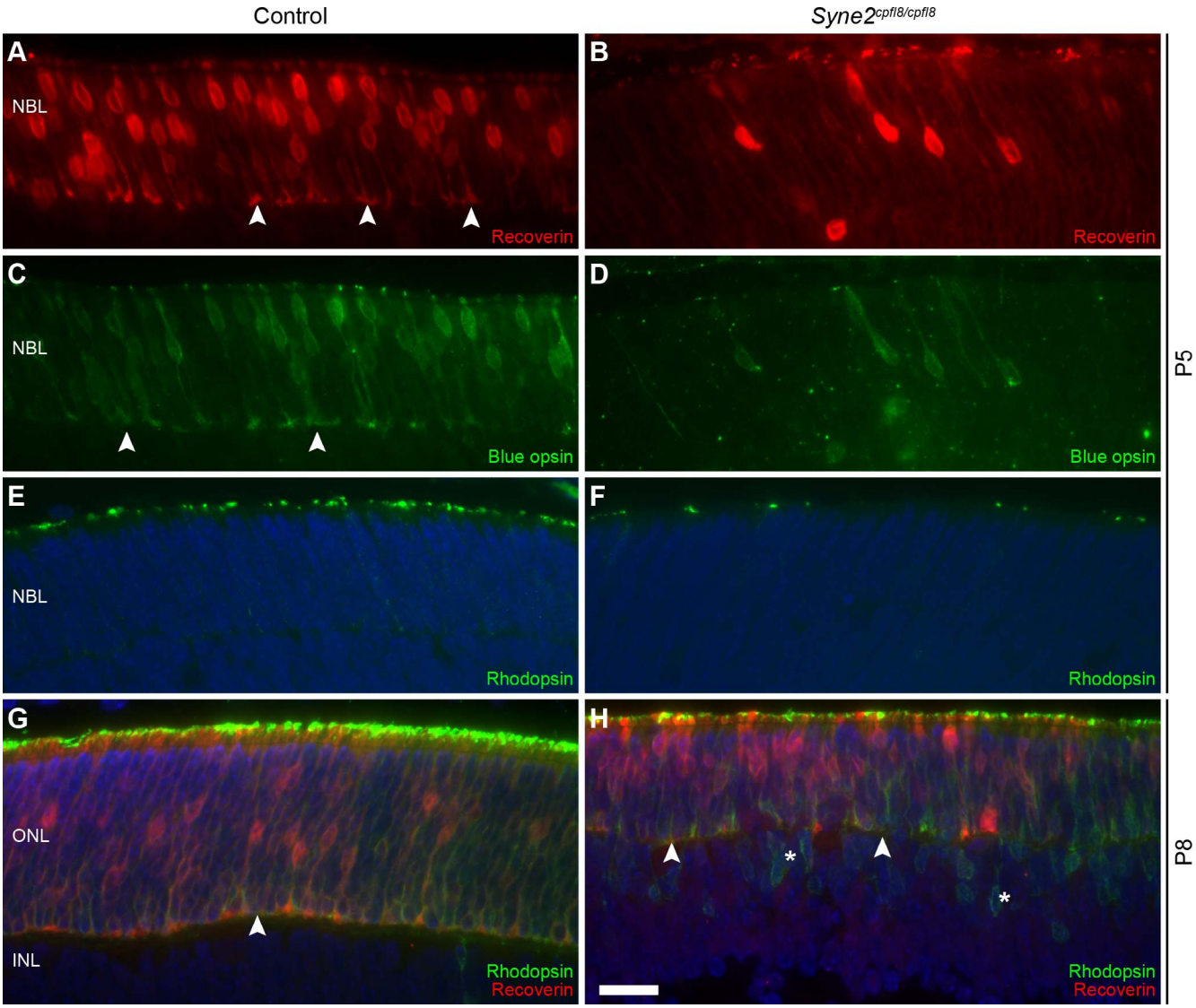

Figure 6. Characterization of the development of photoreceptors in homozygous *Syne2*^{cpfl8} retinas. Staining of P5 neuroblast layer with recoverin ([**A**, **B**] *red*), blue opsin ([**C**, **D**] *green*), and rod opsin ([**E**, **F**] *green*). *Arrows* demarcate photoreceptor cone terminals in B6 control. (**G**, **H**) Colocalization of rhodopsin (*green*) and recoverin (*red*) show rod photoreceptors displaced from their normal position in the ONL to the INL in P8 homozygous *Syne2*^{cpfl8} mutants. *Asterisks* indicate mislocalized rhodopsin-positive cells in the INL. *Scale bars*: 20 μm.

P8, we hypothesized that the misshapen, ectopic cones seen at P5 are removed prior to adulthood; hence, their apparently normal localization at P14 (Fig. 4H). Rhodopsin staining at P5 was restricted to the developing IS-OS region in both mutants and controls (Figs. 6E, 6F). At P8, rhodopsin staining was found throughout the ONL in mutants and controls. Interestingly, homozygous *Syne2*^{cpfl8} retinas exhibited rhodopsin-positive, recoverin-negative staining in cells within the INL (Fig. 6H), presumably corresponding to the mislocalized photoreceptors observed by histological staining (Fig. 3A).

Immunohistochemistry Analysis Reveals Mislocalization of Horizontal, Bipolar, and Müller Cells in Retinas of *Syne2*^{cpfl8} Homozygotes

From the appearance of nuclei in histological sections from eyes of adult mutant mice, we hypothesized that secondary neurons were mislocalized in homozygous *Syne2*^{cpfl8} retinas. To gain a more complete picture of what cell types might be affected in retinas of *Syne2*^{cpfl8} homozygotes, we performed immunofluorescence studies with cell type-specific markers. Calbindin, a marker for horizontal and amacrine cells, stained cell bodies (Figs. 7A, 7C; arrowheads) adjacent to and on the vitreal side of the OPL in wild-type retinas. However, in the *Syne2*^{cpfl8} homozygotes (Figs. 7B, 7D, arrowheads), many horizontal cells were located on the scleral side of the OPL. Additionally, PKCα, a marker for rod bipolar cells, was found on the vitreal side of the OPL (Figs. 7A, 7C, arrowheads) alongside the horizontal cell bodies in controls. However, in the *Syne2*^{cpfl8} homozygotes (Figs. 7B, 7D, white arrows), staining for the bipolar cells were often scattered throughout the INL and occasionally on the scleral side of the OPL. In developing mutant retinas, the horizontal cell terminals appeared thin and disorganized at P8 compared with those in controls (Supplementary Figs. S2A, S2B), and by P14, many cell bodies were positioned toward the scleral side of the OPL

Investigative Ophthalmology & Visual Science

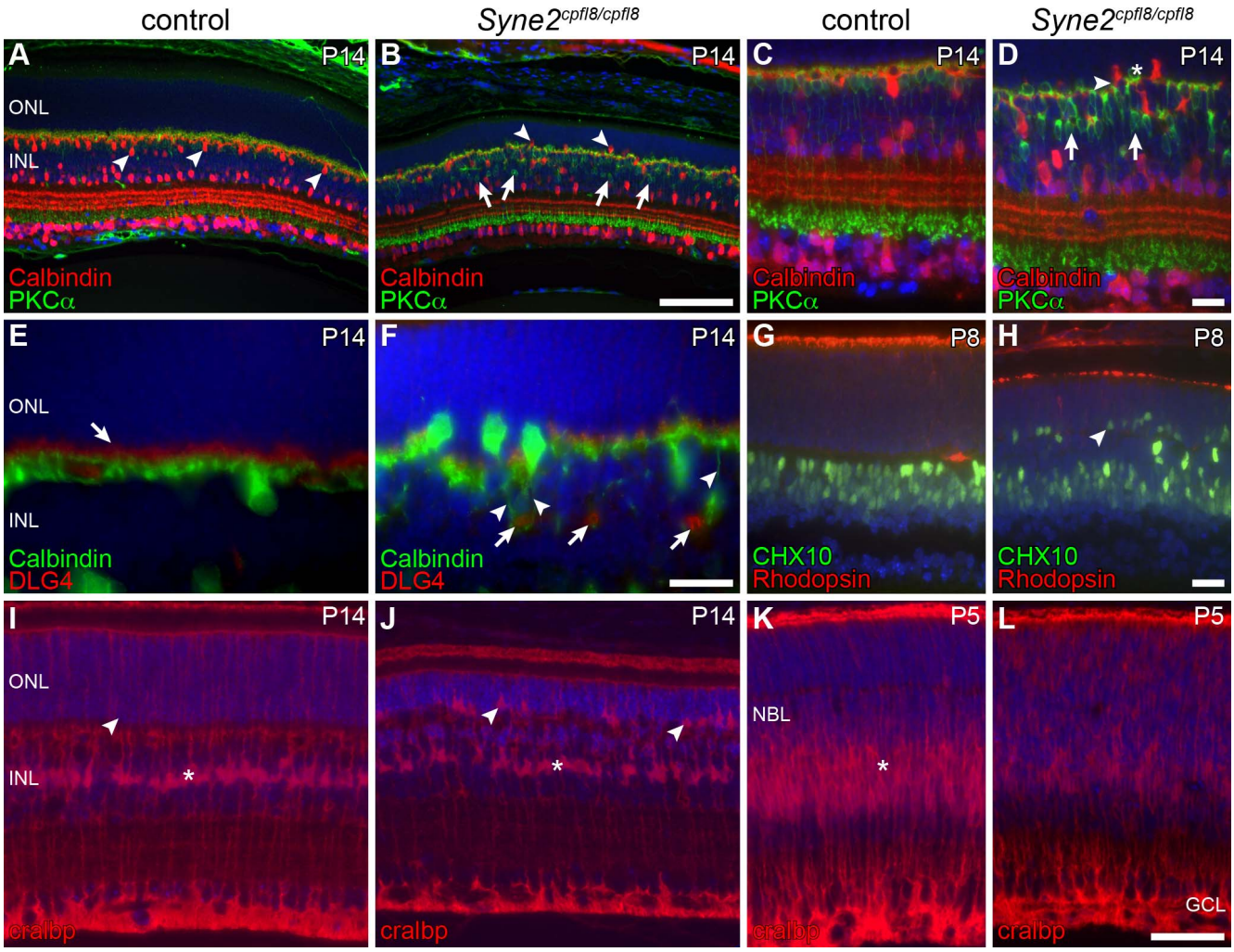

Figure 7. Marker analyses indicate the nature of ectopic cells observed in *Syne2*^{cpfl8} homozygotes at P14. Wild-type (**A**, **C**) and mutants (**B**, **D**) were stained with anti-calbindin (*red*) and anti-PKCα(PRKCA) (*green*) to mark horizontal and bipolar cells, respectively. Displaced horizontal cell bodies (arrowheads) and bipolar cells (arrows: INL and asterisks: scleral side of OPL) are shown in the mutant retinas. (**E**, **F**) Calbindin staining of horizontal cells (*green*) and DLG4 (PSD95) staining of presynaptic terminals in *red* indicate displacement of DLG4-positive presynaptic termini (*arrows*) to the INL and adjacently mislocalized horizontal cells (*arrowheads*). (**G**, **H**) Staining with the bipolar cell marker CHX10 (VSX2) shows early displacement of bipolar cells at P8 in homozygous *Syne2*^{cpfl8} retinas compared to those in B6 controls. (**I**, **J**) Immunostaining with anti-CRALBP (*red*) shows Müller cell somata predominantly in the midzone (*asterisks*) of the INL in wild-type retinas (**I**) at 2 weeks of age. However, in the mutant retinas (**J**), Müller cell somata number are reduced in the INL compared to wild-type. In addition, ectopic Müller cell somata are found at the basal end of the ONL (*white arrowheads*). The corresponding region in B6 retinas is indicated with an *arrow*. (**K**, **L**) At P5, Müller cell bodies (*asterisk*) are restricted to the basal side of the developing OPL in B6 retinas (**K**), whereas Müller cell bodies were dispersed throughout the NBL of the *Syne2*^{cpfl8} homozygotes (**L**). (Note: [**A**, **C**, **E**, **G**, **I**, **K**] are from control mice, whereas [**B**, **D**, **F**, **H**, **J**, **L**] are from mutant mice.) *Scale bars*: 100 μm; (**A**, **B**); 20 μm (**C**–**H**); 50 μm (**I**–**L**).

(Supplementary Figs. S2C, S2D). Labeling with the retinal presynaptic marker DLG4 (formerly PSD95 [Supplementary Figs. S2C, S2D, white arrow]) showed continuous, linear staining in the scleral side of the OPL, immediately adjacent to the ONL in retinas from wild-type controls (Fig. 7E). In contrast, punctate signals for DLG4 normally in the OPL were often observed ectopically in the INL of *Syne2*^{cpfl8} homozygotes (Fig. 7F, white arrows). Also, in some instances, horizontal cell processes (Fig. 7F, arrowheads) could be seen contacting the photoreceptor cells expressing the mislocalized DLG4. Staining with CHX10 (Figs. 7G, 7H) a marker for bipolar cells, revealed that the mutation in *Syne2* leads to an aberrant localization of bipolar cells early in development.

Distribution of the cellular retinaldehyde binding protein (CRALBP/RIBP1), typically present in Müller glia and RPE cells,[22] was examined in the developing retina as well. At P14, Müller cell bodies were uniformly organized midway in the INL in B6 control retinas, whereas a subset of Müller cell bodies were misplaced in the ONL of *Syne2*^{cpfl8} homozygotes (Figs. 7I, 7J). To determine at what developmental stage the mislocalization of the Müller cells occurred, we examined immunostained sections of mutants and controls at P5. At that time point, expression of CRALBP in homozygous *Syne2*^{cpfl8} retinas was found throughout the NBL, whereas in the control retinas, CRALBP expression was found prominently at the basal side of the developing OPL (Figs. 7K, 7L). Likewise, ultrastructural examination revealed abnormalities in the spatial orientation of Müller cells in retinas of adult *cpfl8* mutants. In contrast to Müller cell nuclei in wild-type retinas, which reside exclusively in the INL, several displaced Müller cell nuclei were found in the ONL and OPL of homozygous *Syne2*^{cpfl8} retinas (Supplementary Figs. S2E, S2F).

Investigative Ophthalmology & Visual Science

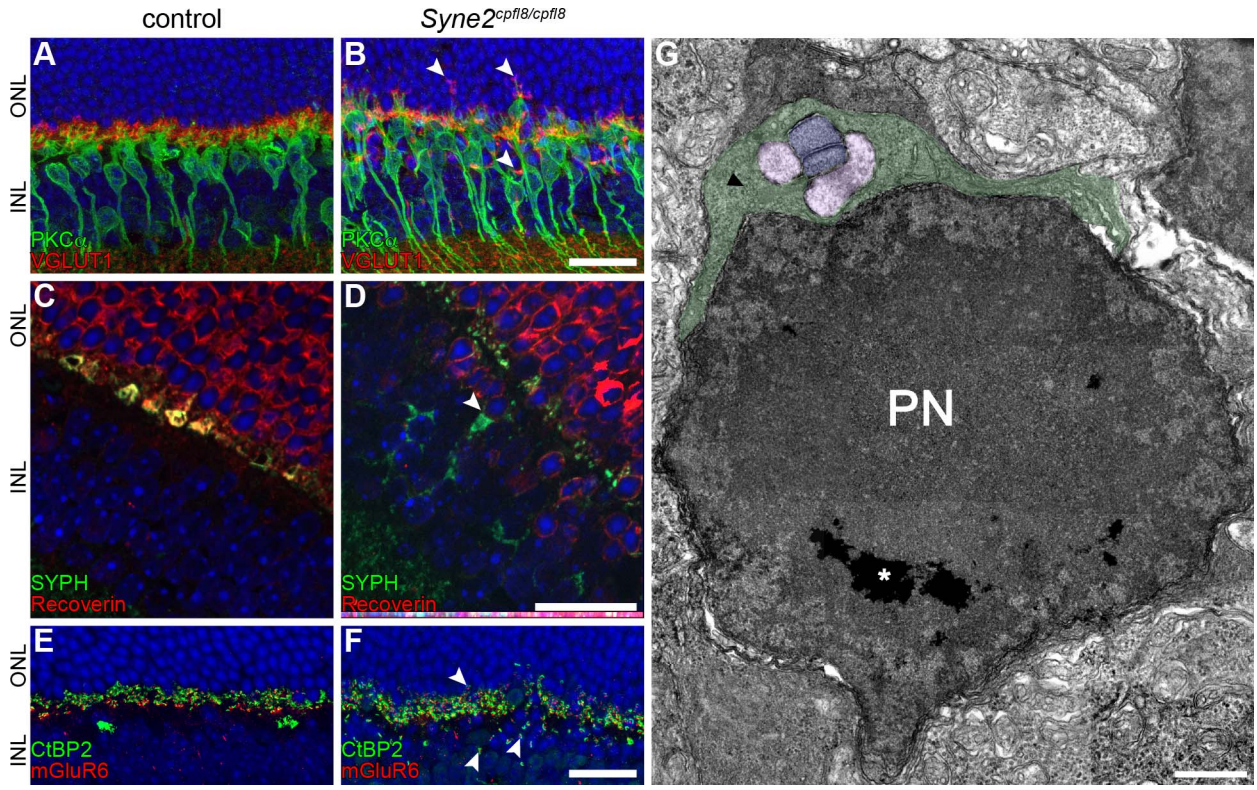

Figure 8. Ectopic synapses in the homozygous *Syne2*^{cpfl8} adult retina. (**A**, **B**) Immunohistochemical staining for the photoreceptor presynaptic molecule VGLUT1(SLC17A7) (*red*) and rod bipolar cells PKCα(PRKCA) (*green*) in wild-type (**A**) and *Syne2*$^{cpfl8/cpfl8}$ (**B**) retinas. Note that rod bipolar cells ectopically extend dendrites into the INL and ONL, and photoreceptor presynaptic terminals are ectopically localized in the INL and ONL of *Syne2*^{cpfl8} homozygotes (*arrowheads*). (**C**, **D**) Staining of control and homozygous *Syne2*^{cpfl8} retinas with the photoreceptor marker recoverin and the presynaptic marker synaptophysin (SYPH). (**E**, **F**) Homozygous *Syne2*^{cpfl8} and control retinas were stained for synaptic ribbons (CTBP2 [*green*]) and the major postsynaptic glutamate receptor (mGluR6/GRM6 [*red*]). Ectopic ribbons are found in close apposition to mGluR6 staining (*arrowheads*). (**G**) Electron microscopy shows an ectopic rod spherule (*green*) contacting two horizontal cell terminals (*pink*) and 1 bipolar cell terminal (*blue*) in the INL of a homozygous *Syne2*^{cpfl8} retina. The synaptic ribbon appears as an electron-dense line (*arrowhead*). PN, photoreceptor nucleus. *Scale bars*: 20 μm (**A**–**F**); 500 nm (**G**).

Ectopic Synapses Appear To Be Structurally Normal in Retinas of *Syne2*^{cpfl8} Homozygotes

In light of the DLG4 localization pattern, we investigated whether synapse formation might be influenced by SYNE2 disruption in *cpfl8* mutant retinas. By immunohistochemical analysis using the photoreceptor presynapse marker vesicular glutamate transporter 1 (VGLUT1 or SLC17A7 [red]) and the bipolar cell marker PKCα (green), ectopic synapses were identified in two locations (Figs. 8A, 8B): within the ONL and within the INL. Costaining by recoverin and synaptophysin (a marker for photoreceptor terminals in the OPL) also showed ectopic synapses in the INL adjacent to mislocalized photoreceptors (Figs. 8C, 8D). To examine the synaptic structure in more detail, we used a marker for the synaptic ribbon, C-terminal binding protein 2 (CTBP2), to visualize the presynaptic region, and the major ON bipolar cell postsynaptic metabotropic glutamate receptor mGluR6 (GRM6) to examine the postsynaptic region (Figs. 8E, 8F). CTBP2 and mGluR6 signals are closely located in ectopic synapses in both INL and OPL, suggesting that interaction between pre and post synapses occurs in ectopic synapses. To further confirm this notion, we performed electron microscopic analysis and found that overall, mislocalized synapses show normal morphology. In the INL and ONL of homozygous *Syne2*^{cpfl8} retinas, ectopic rod spherules were found in contact with horizontal and bipolar cell terminals, and synaptic ribbons were detected and appeared unaffected (Fig. 8G). This observation further supports the notion that ectopically localized photoreceptor terminals synapse with second-order neurons in *cpfl8* mice.

Discussion

In the present study, we reviewed and extended earlier findings of photoreceptor INM defects in the new *Syne2* model *cpfl8*. This spontaneous, recessive mutation results in the loss of a high-molecular-weight isoform of SYNE2 thought to be associated with the nuclear migration of retinal neurons during the early phases of retinogenesis.[18] Like a previously described *Syne2*$^{-/-}$ null mutant,[13] homozygous *Syne2*^{cpfl8} mutants exhibit an abnormal cone and rod ERG phenotype and mislocalization of rod photoreceptors in the INL.

Furthermore, secondary neurons (rod bipolar and horizontal cells) and Müller glia are also displaced in homozygous *Syne2*^{cpfl8} retinas. These effects are not unexpected, as *Syne2* is highly expressed in the INL and GCL during retinal development and in adult retinas.[13,18] Mislocalization of secondary neurons and Müller glia may result directly from INM defects associated with *Syne2*^{cpfl8} in neuroepithelial progenitor cells, which give rise to rod bipolar and horizontal cells, or in multipotent progenitors, which differentiate into Müller cells during the first postnatal week, respectively.[23,24] Support for this idea comes from the observation that in zebrafish, INM occurs in Müller glia, where it is an important response to retinal injury.[25] Alternatively, mislocalization of

cells in *Syne2*^{cpfl8} homozygotes may be an indirect consequence of retinal remodeling in response to abnormal neuronal development. Müller cells may migrate in response to the extensive neuronal apoptosis in homozygous *Syne2*^{cpfl8} mice at P5, similar to their translocation toward the outer retina upon photoreceptor injury.[26] Displacement of the horizontal cells may be explained by their remarkable plasticity and ability to migrate freely when connections to neighboring photoreceptors are disrupted.[27]

The *Syne2*^{cpfl8} model shows a decrease in amplitude of the ERG b-wave, which may reflect a reduction in the number of photoreceptor cells and/or abnormalities in synaptic transmission. However, interestingly, transgenic overexpression of the EGFP-KASH domain in photoreceptors, aimed to disrupt the LINC complexes of which SYNE2 is an integral part, demonstrated mislocalization of cone photoreceptors with no effects on photoreceptor number or function.[17] This suggests that the *Syne2*^{cpfl8} ERG b-wave phenotype must be caused by nonphotoreceptor cell factors, such as the observed, aberrant localization of secondary neurons. Mislocalization of secondary neurons results in ectopic synapse formation in both the ONL and INL of homozygous *Syne2*^{cpfl8} retinas. Ectopic synapses in the ONL have been observed in a number of mouse models with mutations in presynaptic components that are involved in neurotransmission in the retina,[28–33] which also result in a decrease or loss in ERG b-wave.

A subset of cones failed to form in developing retinas of *Syne2*^{cpfl8} homozygotes. The reduced number of cone cells results from both a decreased number of developing cells and increased cell death, peaking at P5. Strikingly, at P5, developing cone photoreceptors do not form properly elongated axons and terminals. Roles in axonal outgrowth and termination have recently been described in the worm ortholog of SYNE2, Anchorage 1 (ANC1).[34] ANC1 is a member of the highly conserved Pam/Highwire/RPM-1 (PHR) family of signaling molecules and is thought to regulate synapse formation and axon termination via a β-catenin/armadillo-related protein (BAR1) pathway. PHR1, a neuronal signaling molecule upstream of SYNE2, is required for the proper arborization of retinal axons in zebrafish.[35] Recent studies have shown that SYNE2 forms a complex with α,β-catenin and emerin and thereby plays a role in the regulation of nuclear β-catenin expression and WNT signaling at the nuclear envelope.[36] Altogether, these observations lead us to speculate that perhaps, in addition to its function in neuronal migration, SYNE2 may play an important role in the outgrowth and termination of mammalian cone axons during photoreceptor development.

Results from this study extend our understanding of SYNE2 function in the murine retina: its roles in cone cell neurogenesis and nuclear migration of neuroepithelial progenitor cells and its influence on positioning of photoreceptors, secondary neurons, and Müller glia during early development. Future study of mutations affecting SYNE2 and other LINC complex members has great potential in furthering our understanding of INM during mammalian retinal development.

Acknowledgments

The authors thank Jeanie Hansen, Jeremy Charette, Jungyeon Won, PhD, Ye Liu, PhD, and Lihong Zhao, PhD, for excellent technical assistance. Initial mapping of the *cpfl8* mutation was performed by the Fine Mapping Laboratory, Scientific Services Department, the Jackson Laboratory.

Supported by US National Institutes of Health Grants EY011996 (PMN), EY016501 (PMN), EY016313 (DMM), EY022086 (AI), HD007065 (CHP), and NSF Grant MCB0817787 (LSS). Shared scientific services are supported in part by National Cancer Institute Cancer Center Support Grant CA34196.

Disclosure: **D.M. Maddox**, None; **G.B. Collin**, None; **A. Ikeda**, None; **C.H. Pratt**, None; **S. Ikeda**, None; **B.A. Johnson**, None; **R.E. Hurd**, None; **L.S. Shopland**, None; **J.K. Naggert**, None; **B. Chang**, None; **M.P. Krebs**, None; **P.M. Nishina**, None

References

1. Apel ED, Lewis RM, Grady RM, Sanes JR. Syne-1, a dystrophin- and Klarsicht-related protein associated with synaptic nuclei at the neuromuscular junction. *J Biol Chem*. 2000;275:31986–31995.
2. Zhang Q, Ragnauth C, Greener MJ, Shanahan CM, Roberts RG. The nesprins are giant actin-binding proteins, orthologous to *Drosophila melanogaster* muscle protein MSP-300. *Genomics*. 2002;80:473–481.
3. Crisp M, Liu Q, Roux K, et al. Coupling of the nucleus and cytoplasm: role of the LINC complex. *J Cell Biol*. 2006;172:41–53.
4. Zhang Q, Skepper JN, Yang F, et al. Nesprins: a novel family of spectrin-repeat-containing proteins that localize to the nuclear membrane in multiple tissues. *J Cell Sci*. 2001;114:4485–4498.
5. Meinke P, Nguyen TD, Wehnert MS. The LINC complex and human disease. *Biochem Soc Trans*. 2011;39:1693–1697.
6. Zhang Q, Bethmann C, Worth NF, et al. Nesprin-1 and -2 are involved in the pathogenesis of Emery Dreifuss muscular dystrophy and are critical for nuclear envelope integrity. *Hum Mol Genet*. 2007;16:2816–2833.
7. Zhang X, Xu R, Zhu B, et al. Syne-1 and Syne-2 play crucial roles in myonuclear anchorage and motor neuron innervation. *Development*. 2007;134:901–908.
8. Luke Y, Zaim H, Karakesisoglou I, et al. Nesprin-2 Giant (NUANCE) maintains nuclear envelope architecture and composition in skin. *J Cell Sci*. 2008;121:1887–1898.
9. Kracklauer MP, Banks SM, Xie X, Wu Y, Fischer JA. *Drosophila* klaroid encodes a SUN domain protein required for Klarsicht localization to the nuclear envelope and nuclear migration in the eye. *Fly (Austin)*. 2007;1:75–85.
10. Patterson K, Molofsky AB, Robinson C, Acosta S, Cater C, Fischer JA. The functions of Klarsicht and nuclear lamin in developmentally regulated nuclear migrations of photoreceptor cells in the *Drosophila* eye. *Mol Biol Cell*. 2004;15:600–610.
11. Tsujikawa M, Omori Y, Biyanwila J, Malicki J. Mechanism of positioning the cell nucleus in vertebrate photoreceptors. *Proc Natl Acad Sci U S A*. 2007;104:14819–14824.
12. Del Bene F, Wehman AM, Link BA, Baier H. Regulation of neurogenesis by interkinetic nuclear migration through an apical-basal notch gradient. *Cell*. 2008;134:1055–1065.
13. Yu J, Lei K, Zhou M, et al. KASH protein Syne-2/Nesprin-2 and SUN proteins SUN1/2 mediate nuclear migration during mammalian retinal development. *Hum Mol Genet*. 2011;20:1061–1073.
14. Zhang X, Lei K, Yuan X, et al. SUN1/2 and Syne/Nesprin-1/2 complexes connect centrosome to the nucleus during neurogenesis and neuronal migration in mice. *Neuron*. 2009;64:173–187.
15. Baye LM, Link BA. Nuclear migration during retinal development. *Brain Res*. 2008;1192:29–36.
16. Spear PC, Erickson CA. Interkinetic nuclear migration: a mysterious process in search of a function. *Dev Growth Differ*. 2012;54:306–316.
17. Razafsky D, Blecher N, Markov A, Stewart-Hutchinson PJ, Hodzic D. LINC complexes mediate the positioning of cone photoreceptor nuclei in mouse retina. *PLoS One*. 2012;7:e47180.

18. Razafsky DS, Ward CL, Kolb T, Hodzic D. Developmental regulation of linkers of the nucleoskeleton to the cytoskeleton during mouse postnatal retinogenesis. *Nucleus*. 2013;4:399–409.
19. Nusinowitz S, Ridder WHI, Heckenlively JR. Electrophysiological testing of the mouse visual system. In: Smith RS, John SWM, Nishina PM, Sundberg JP, eds. *Systematic Evaluation of the Mouse Eye: Anatomy, Pathology and Biomethods*. New York: CRC Press; 2002:320–344.
20. Schindelin J, Arganda-Carreras I, Frise E, et al. Fiji: an open-source platform for biological-image analysis. *Nat Methods*. 2012;9:676–682.
21. Broedersz CP, Brangwynne CP. Nuclear mechanics: lamin webs and pathological blebs. *Nucleus*. 2013;4:156–159.
22. Saari JC, Crabb JW. Focus on molecules: cellular retinaldehyde-binding protein (CRALBP). *Exp Eye Res*. 2005;81:245–246.
23. Turner DL, Cepko CL. A common progenitor for neurons and glia persists in rat retina late in development. *Nature*. 1987; 328:131–136.
24. Rich KA, Figueroa SL, Zhan Y, Blanks JC. Effects of Muller cell disruption on mouse photoreceptor cell development. *Exp Eye Res*. 1995;61:235–248.
25. Goldman D. Muller glial cell reprogramming and retina regeneration. *Nat Rev Neurosci*. 2014;15:431–442.
26. Joly S, Pernet V, Samardzija M, Grimm C. Pax6-positive Muller glia cells express cell cycle markers but do not proliferate after photoreceptor injury in the mouse retina. *Glia*. 2011;59: 1033–1046.
27. Poche RA, Reese BE. Retinal horizontal cells: challenging paradigms of neural development and cancer biology. *Development*. 2009;136:2141–2151.
28. Dick O, tom Dieck S, Altrock WD, et al. The presynaptic active zone protein bassoon is essential for photoreceptor ribbon synapse formation in the retina. *Neuron*. 2003;37:775–786.
29. Haeseleer F, Imanishi Y, Maeda T, et al. Essential role of Ca2+-binding protein 4, a Cav1.4 channel regulator, in photoreceptor synaptic function. *Nat Neurosci*. 2004;7:1079–1087.
30. Claes E, Seeliger M, Michalakis S, Biel M, Humphries P, Haverkamp S. Morphological characterization of the retina of the CNGA3(-/-)Rho(-/-) mutant mouse lacking functional cones and rods. *Invest Ophthalmol Vis Sci*. 2004;45:2039–2048.
31. Chang B, Heckenlively JR, Bayley PR, et al. The nob2 mouse, a null mutation in Cacna1f: anatomical and functional abnormalities in the outer retina and their consequences on ganglion cell visual responses. *Vis Neurosci*. 2006;23:11–24.
32. Morgans CW, Bayley PR, Oesch NW, Ren G, Akileswaran L, Taylor WR. Photoreceptor calcium channels: insight from night blindness. *Vis Neurosci*. 2005;22:561–568.
33. Mansergh F, Orton NC, Vessey JP, et al. Mutation of the calcium channel gene Cacna1f disrupts calcium signaling, synaptic transmission and cellular organization in mouse retina. *Hum Mol Genet*. 2005;14:3035–3046.
34. Tulgren ED, Turgeon SM, Opperman KJ, Grill B. The Nesprin family member ANC-1 regulates synapse formation and axon termination by functioning in a pathway with RPM-1 and beta-catenin. *PLoS Genet*. 2014;10:e1004481.
35. D'Souza J, Hendricks M, Le Guyader S, et al. Formation of the retinotectal projection requires Esrom, an ortholog of PAM (protein associated with Myc). *Development*. 2005;132:247–256.
36. Neumann S, Schneider M, Daugherty RL, et al. Nesprin-2 interacts with α-catenin and regulates Wnt signaling at the nuclear envelope. *J Biol Chem*. 2010;285:34932–34938.

Investigative Ophthalmology & Visual Science